Polymer 55 (2014) 6439–6443

Contents lists available at ScienceDirect

Polymer

journal homepage: www.elsevier.com/locate/polymer

Polymer communication

Nanovoid morphology and distribution in deformed HDPE studied by magnified synchrotron radiation holotomography

Thilo F. Morgeneyer [a, *], Henry Proudhon [a], Peter Cloetens [b], Wolfgang Ludwig [b, c], Quentin Roirand [a], Lucien Laiarinandrasana [a], Eric Maire [c]

[a] MINES ParisTech, PSL Research University, MAT – Centre des matériaux, CNRS UMR 7633, BP 87, 91003 Evry, France
[b] European Synchrotron Radiation Facility (ESRF), BP 220, F-38043 Grenoble Cedex, France
[c] Universite de Lyon, INSA-Lyon, MATEIS CNRS UMR5510, 7 Avenue Jean Capelle, 69621 Villeurbanne, France

ARTICLE INFO

Article history:
Received 12 September 2014
Received in revised form
23 September 2014
Accepted 5 October 2014
Available online 15 October 2014

Keywords:
HDPE
Nano-cavities
Magnified synchrotron holotomography

ABSTRACT

The individual morphology and size distribution of nano-cavities in a necked tensile specimen made of semicrystalline high-density polyethylene (HDPE) have been observed and quantified in three dimensions using magnified synchrotron radiation holotomography. Here, using a voxel size of 59.7 nm, permanent voids in the unloaded state after yielding are observed that can only be assessed in averaged manner at finer length scales using small angle X-ray scattering (SAXS) techniques. Observation of the same sample using typical synchrotron radiation tomography with micron resolution is also given highlighting the novel opportunities arising with magnified synchrotron radiation holotomography in comparison. Two populations of voids elongated in loading direction are observed: A population of large cavities that has nucleated around inclusions and a population of small cavities. All cavities are equiaxed in radial directions and elongated in loading direction which is consistent with SAXS findings of other studies. Void volume fraction, void size distributions and characteristic dimensions of the voids are assessed using 3D image analysis.

1. Introduction

Damage and cavitation in semicrystalline polymers during deformation and necking has been investigated in various studies in the past, attributing sample whitening to cavitation [1–3]. Both SAXS and WAXS techniques have widely been used to investigate the nucleation of cavities and their shape in HDPE at length scales of tens of nanometres [4–8]. The cavities are initially oriented normal to the deformation direction and then change their orientation along the deformation direction with a microstructure evolution from lamellae to fibrillar texture [9]. The thinning and elongation of voids during straining in HDPE have been observed [10], and it has been reported that during the process of lamellar to fibrillar transition, intralamellar slips of the crystalline blocks are activated at low deformations, followed by stress-induced fragmentation of the crystal blocks which is also reported in Ref. [11] as deformation process.

Damage in semicrystalline polymers has recently been studied via synchrotron radiation computed tomography (SRCT). Blaise et al. observed cavitation in HDPE and applied 2D Fast Fourier Transform analysis to reconstruct tomographic sections to determine damage anisotropy [12]. The size of the damage features in this study was however close to the resolution limit. At the same time, Laiarinandrasana et al. observed larger damage features in the neck of a tested smooth Polyamide 6 (PA6) specimen via SRCT [13]. Damage in the form of voids aligned in columns along the deformation direction (height of the columns ~50 μm) separated by ligaments of solid polymer has been observed and confirmed by cryofractography technique. In Ref. [13] the evolution of damage in PA6 and the effect of stress triaxiality and loading/unloading on cavitation have been assessed via SRCT. Tomography is also used in other studies to obtain average damage values in polyvinylidene difluoride (PVDF) [14].

In the present work, the spatial distribution of damage in a necked tensile HDPE specimen is assessed via magnified holotomography allowing for unprecedented insights into nanovoid shape neither directly accessible via SAXS techniques (as these are averaged measurements) nor via cryofractography due to the low T_g of HDPE and its softness at room temperature. The void shape and size distributions are quantified via 3D image analysis.

* Corresponding author.
E-mail address: thilo.morgeneyer@ensmp.fr (T.F. Morgeneyer).

http://dx.doi.org/10.1016/j.polymer.2014.10.022
0032-3861/

2. Experimental section

The material is an Irgafos 168 polyethylene which includes carbon black. The density value is close to 0.943 (also see Table 1 for further material information). The samples were cut out from injected moulded plates [15].

Fig. 1 shows an SEM micrograph of the microstructure after permanganic etching. The lamellar structure of the spherulite becomes evident. The spherulite shown here has a diameter of about 4 μm. An average diameter of about 2 μm has been estimated using several micrographs. The white particles on the surface are believed to be carbon black particles [16]. These particles may act as nucleation site for voids.

The mechanical tensile test has been carried out using a displacement controlled electro-mechanical testing machine. An axi-symmetric specimen with an initial diameter of 3 mm and a gauge length of 15 mm was used. The specimen outer ends were rectangular (see Fig. 2). The crosshead displacement speed was 0.015 mm/s. The engineering stress versus crosshead displacement curve is given in Fig. 2. Necking started at peak load. The test has been stopped after some neck extension and the specimen has been unloaded. The diameter of the unloaded neck was 1.5 mm giving an approximate radial strain of 50%. The tomography scanning has been carried out 7 months after the tensile experiment which means that only permanent damage could be observed.

For the first observation, standard parallel beam synchrotron radiation tomography has been carried out at the European Synchrotron Radiation Facility (ESRF), beamline ID19. As a reminder, tomography, analogue to the better known X-ray medical scanner, is based on the acquisition of many transmission X-ray radiographies, while the samples rotate [17]. From the composition of this set of images, using an appropriate computed algorithm, it is possible to calculate the 3D spatial distribution of the X-ray attenuation inside the sample, providing an image of the density distribution and thus of the internal microstructure non-destructively. In our case, an energy of 19 keV and a voxel size of 0.7 μm have been used (similar condition as in Ref. [13]) and the total scanned volume was 1 mm^3. In terms of spatial resolution parallel beam synchrotron tomography is limited by the performances of the detector (see Fig. 3). In the best cases, this limit cannot go easily below 0.5 μm. This resolution limit might not be good enough to allow us to visualize very fine damage features of our material.

To overcome this limitation, magnified holotomography has been developed in the last ten years on the ESRF beamline ID22NI [18]. The principle of this improvement is to create an intense and divergent X-ray beam and to use the divergence to magnify the projections by simply moving a classical detector (2 μm pixel size can be enough) away from the focal point (see Fig. 3). This practical way of obtaining a high resolution, is already used in conical standard laboratory tomographs. It is known that, because of a phenomenon named *geometric blur*, in this case of diverging magnification, the limiting physical factor for the resolution is the finite size of the focal point from where the X-rays are generated. In standard divergent X-ray tubes, this size can hardly be smaller than 1 micron, and in this case of very small spot size, the intensity of the emitted X-rays is rather weak, leading to long exposure times and small signal to noise ratios.

Table 1
HDPE material characteristics: Index of crystallinity (X_C), weight average molar mass (Mw), polydispersity index (Ip), carbon black content (after Ref. [15]).

X_C	Mw	Ip	Carbon black content
55%	203 kg/mol	20.3	2.2%

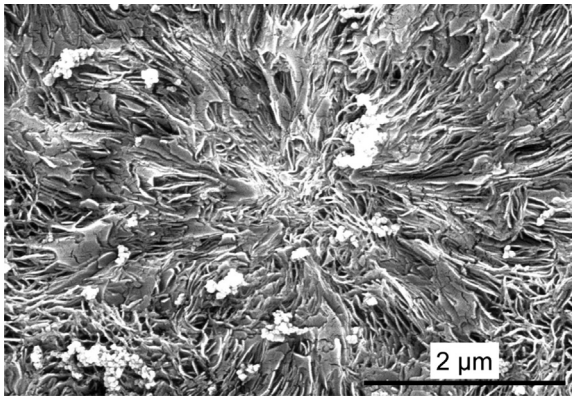

Fig. 1. SEM micrograph of a spherulite after permanganic-etching.

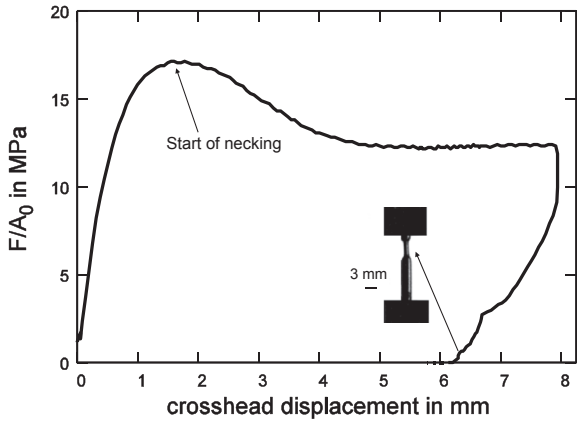

Fig. 2. Nominal stress versus crosshead displacement curve for the tensile test and picture of the necked specimen in unloaded state (F = load, A_0 = initial cross section).

X-rays are known to be hard to focus but with the recent rapid advances in X-ray optics, this concept can now be used with synchrotron sources as well. In this study, we have used a set-up where a Kirkpatrick-Baez optics system focuses the initially parallel synchrotron beam down to a focal spot below 100 nm in lateral size. The multilayer coated optics also selects from the initially pink beam a narrow energy band around 16.9 keV. In the case of the very coherent initial synchrotron beam used here, the amount of phase contrast in the projection with such a long propagation distance is enormous. This implies that simple attenuation is not the only

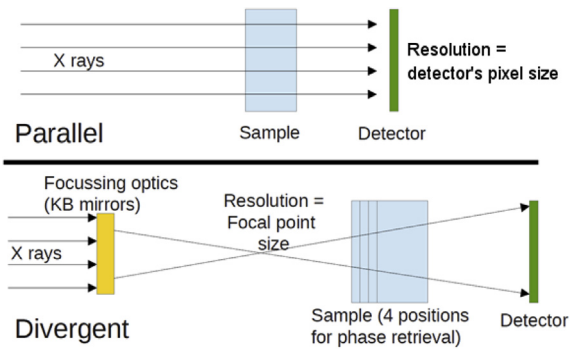

Fig. 3. Top: classical synchrotron radiation computed tomography setup with micrometre resolution; bottom: magnified holotomography setup allowing for resolution up to tens of nanometres.

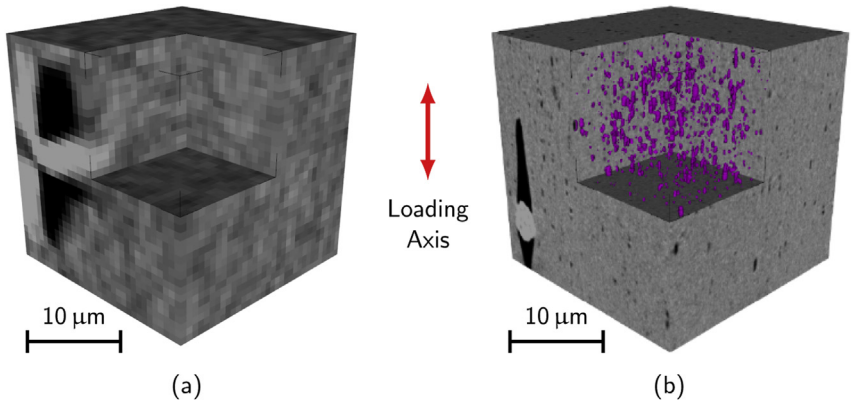

Fig. 4. 3D cubes showing a pair of big voids nucleated at an inclusion seen by (a) micro-tomography (voxel size 0.7 μm) versus, b) magnified holotomography (voxel size 59.7 nm).

source of contrast in the obtained images and phase retrieval by holotomography is a compulsory step of the reconstruction on beamline ID22NI. Each holotomography scan was composed of four tomography acquisitions at different distances between the focal point and the sample. For tomography acquisition, 2000 projections were acquired over 360° and the exposure time per frame was 0.25 s. The final reconstructed volume was a cylinder of 150 μm in height and 150 μm in diameter. More details on the set-up can be found in Ref. [19]. Examples of the use of this set-up in the field of materials science have been published in Refs. [18,20,21].

The deformed HDPE specimen of this study has been observed in the central part of the neck at beamline ID22NI at the European Synchrotron Radiation Facility (ESRF) with a voxel size of 59.7 nm.

All 3D image cubes were visualized using python scripts and the VTK library. Part of the cube is clipped away to reveal nanovoids using grey level thresholding. For 3D image analysis, a set of in-house python routines was used. A 1024 × 1024 × 1024 voxel cube was used as volume element (about $(60\ \mu m)^3$) for void and particle analysis. Voids and particles were segmented applying a simple thresholding method (see Fig. 5). Voids could then be labelled and the size distributions readily calculated.

3. Results and discussion

Both images in Fig. 4 depict a $(24\ \mu m)^3$ volume of material at different spatial resolutions: Fig. 4(a) shows tomography data that provides micrometre resolution. The pseudo 3D cube of damaged material in the neck shows pairs of voids (black) that are likely to have nucleated at the inclusion. This nucleation occurs by particle matrix decohesion at each of the two poles of the inclusions. The

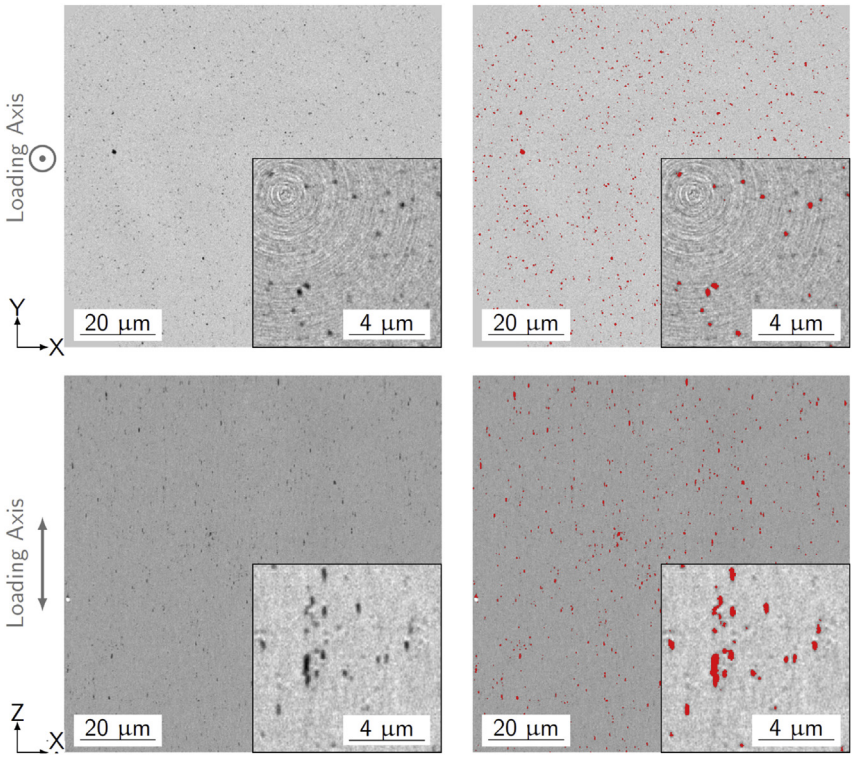

Fig. 5. 2D sections of reconstructed magnified holotomography data; left: raw sections, right: overlay of raw section and segmented voids in red; the insets display higher magnification of the images. (For interpretation of the references to colour in this figure legend, the reader is referred to the web version of this article.)

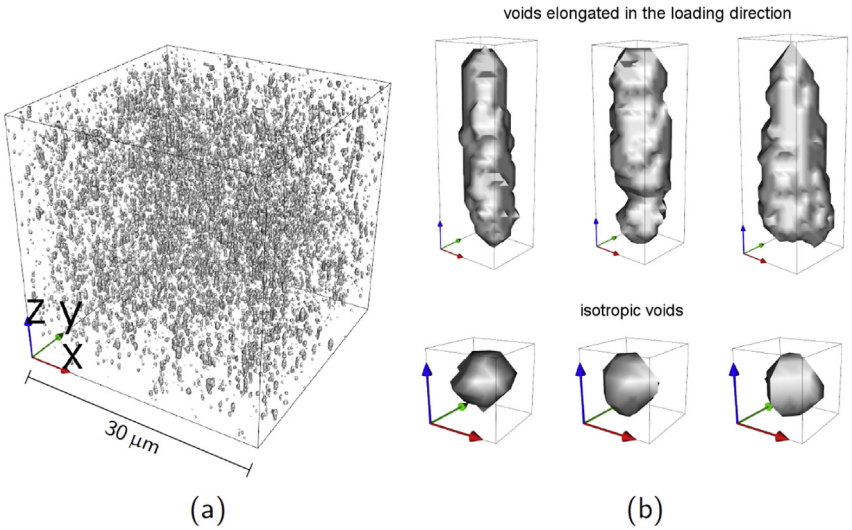

Fig. 6. 3D visualization of cavities within the material; (a) all cavities in a representative volume of 30 $(\mu m)^3$, (b) typical cavities (both elongated and isotropic) are shown with a high magnification (the arrow length is 0.3 µm here).

subsequent growth of the nucleated cavities leads to the observed shape in Fig. 4. This observation is seen at many places in the dataset.

In Fig. 4(b), a pseudo 3D cube of magnified holotomography, that achieves voxel sizes of 59.7 nm, is shown. Two main populations of voids can be clearly distinguished with this improved resolution: large voids around an inclusion and elongated in the loading direction are observed similarly to that seen via more classical tomography in Fig. 4(a). Another population of much smaller voids can now be observed in the polymer matrix with a length ranging from 100 nm to 1 µm. This population is also elongated in the loading direction which is consistent with previous results from the literature using SAXS techniques [8,9] that allow to investigate the morphological distribution of voids indirectly at smaller length scales and at earlier stages of deformation and damage. In these studies voids are shown to be initially nucleated in the form of platelets normal to the loading direction and then elongate in loading direction because of void growth with further straining. This mechanism is also found for other semi-crystalline polymers with larger spherulite sizes [13,22]. Two void populations have also been detected via tomography in Ref. [12], but the shape of the small voids could not be resolved. It is possible that voids at even smaller scales are present here that are not observable with the present technique. Several bigger voids appear in pairs as if they had nucleated around a particle, which could be carbon black. The exact nature of the particle remains difficult to identify.

Previous observations in Ref. [13] for PA6 and in Ref. [22] for polypropylene (PP) showed that voids are aligned in columns. However, for the present material (HDPE) the void columns, seen for PA6 and PP, are less clearly discernible. This may either be due to the absence of such features, to the fact that they appear at smaller length scales or the fact that they may substantially stretch and close during subsequent straining.

Fig. 5 left shows typical 2D sections of magnified holotomography data normal to the loading direction for the upper image and normal to the specimen radius for the lower image. In Fig. 5 right an overlay of the segmented voids (in red) on the initial reconstructed data is given.

The void volume fraction for the chosen threshold value corresponds to 1.2% (voids smaller than 8 voxels are not accounted for). An unambiguous measurement of a void volume fraction is challenging as it cannot be entirely ascertained that the voids are empty. A certain amount of fibrils, as typically found in crazes, may still be present in the cavity and contribute to a brighter grey value [23]. In Fig. 6(a) a 3D cube is given showing a 3D rendering of the voids. In Fig. 6(b) zooms on isotropically shaped cavities and cavities elongated in loading direction are given. It can be seen that the elongated voids have a larger volume than the isotropic ones.

Individual void shapes are characterized using the Feret dimensions (smaller inclusive bounding box) along all three directions *X*, *Y*, and *Z* (=loading direction). Fig. 7 shows the

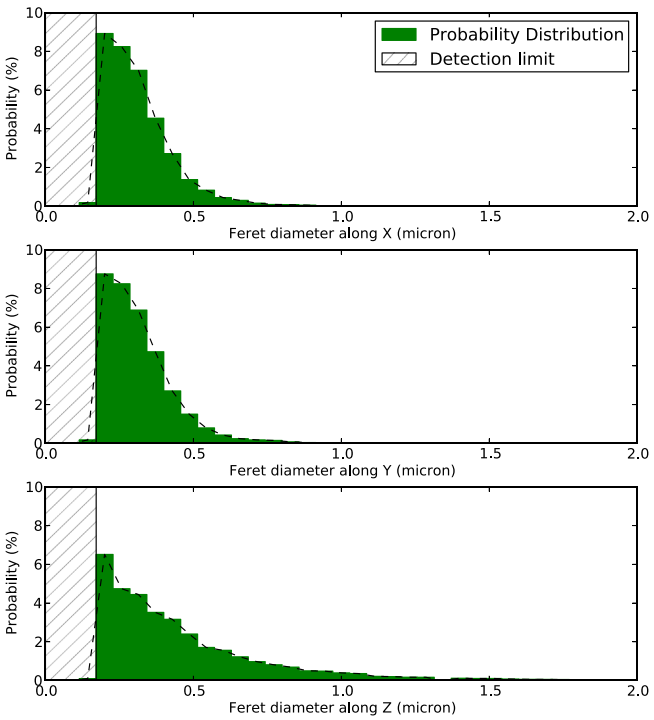

Fig. 7. 3D size analysis of the cavities, the size distribution along the *X* and *Y* axes are identical (the cavities are transversely isotropic) whereas the distribution along the loading axis extends much further showing that many cavities are elongated in this direction.

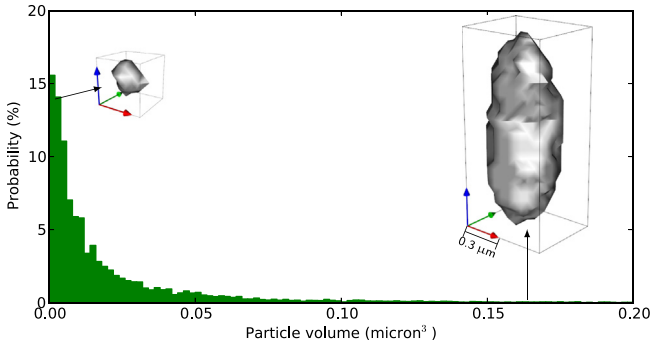

Fig. 8. Volume histogram of cavities as measured by magnified holotomography. Small cavities tend to be rather spherical while large ones appear elongated in the loading direction.

distribution of the voids Feret dimensions. The size distribution for *X* and *Y* directions is very similar and centred around 0.3 μm. For the *Z* direction, the peak is at a slightly higher value and the distribution is substantially broader indicating that the voids are elongated in loading direction which is consistent with SAXS for large deformations [10]. The void size distribution (Fig. 8) shows a peak of voids at the smallest detectable volume (0.0017 μm^3). This indicates that there may be voids at even smaller length scales. Such an effect of the resolution on void detection has for example already been observed in Ref. [24]. The distribution spreads out to volumes as large as 1 μm^3. A more careful observation of the individual voids shows that spherical voids are very numerous and small ($\leq$0.01 μm^3) and as the volume increases, the voids are more and more elongated in the loading direction but also grow in the lateral directions. This may imply that large voids have nucleated early and grown in loading direction whereas the round voids nucleated later and are in earlier stages of growth.

4. Concluding remarks

In summary, it could be shown that magnified holotomography has a great potential of assessing polymer microstructures and their evolution at nanometric scales in the 3D material bulk in a non-destructive manner. A broad size distribution of voids was found. Some big voids have nucleated at heavy particles and a population of smaller equiaxed voids with different sizes is seen everywhere in the matrix. Both are elongated in loading direction which is consistent with SAXS findings from the literature for states of large deformation. The smaller voids are not discernible with classical tomography techniques. The measured void volume fraction is low (~1%) compared to other semi-crystalline polymers (~20% for PA6).

Acknowledgements

We would like to acknowledge ESRF for beamtime in experiment MA1003 and we would like to thank Heikki Suhonen for his help in Magnified Synchrotron Radiation Holotomography observation.

References

[1] Gehant S, Schirrer R. Multiple light scattering and cavitation in two phase tough polymers. J Polym Sci Part B Polym Phys 1999;37(2):113–26.
[2] Kambour RP. A review of crazing and fracture in thermoplastics. J Polym Sci Macromol Rev 1973;7(1):1–154.
[3] Pawlak A, Galeski A, Rozanski A. Cavitation during deformation of semi-crystalline polymers. Prog Polym Sci 2014;39(5):921–58.
[4] Young P, Kyu T, Suehiro S, Lin J, Stein R. Dynamic small-angle X-ray-scattering from crystalline polymers. J Polym Sci Part B Polym Phys 1983;21(6):881–92.
[5] Butler M, Donald A, Ryan A. Time resolved simultaneous small- and wide-angle X-ray scattering during polyethylene deformation 2. Cold drawing of linear polyethylene. Polymer 1998;39(1):39–52.
[6] Pawlak A, Galeski A. Plastic deformation of crystalline polymers: the role of cavitation and crystal plasticity. Macromolecules 2005;38(23):9688–97.
[7] Pawlak A, Galeski A. Cavitation during tensile deformation of polypropylene. Macromolecules 2008;41(8):2839–51.
[8] Humbert S, Lame O, Chenal JM, Rochas C, Vigier G. New insight on initiation of cavitation in semicrystalline polymers: in-situ SAXS measurements. Macromolecules 2010;43(17):7212–21.
[9] Pawlak A. Cavitation during tensile deformation of high-density polyethylene. Polymer 2007;48(5):1397–409.
[10] Jiang Z, Tang Y, Rieger J, Enderle H-F, Lilge D, Roth SV, et al. Two lamellar to fibrillar transitions in the tensile deformation of high-density polyethylene. Macromolecules 2010;43(10):4727–32.
[11] Strobl G. The physics of polymers. Springer; 2007.
[12] Blaise A, Baravian C, Andre S, Dillet J, Michot LJ, Mokso R. Investigation of the mesostructure of a mechanically deformed HDPE by synchrotron micro-tomography. Macromolecules 2010;43(19):8143–52.
[13] Laiarinandrasana L, Morgeneyer TF, Proudhon H, N'guyen F, Maire E. Effect of multiaxial stress state on morphology and spatial distribution of voids in deformed semi-crystalline polymer assessed by X-ray tomography. Macromolecules 2012;45:4658–68.
[14] Rosenberg E, Brusselle-Dupend N, Epsztein T. A mesoscale quantification method of cavitation in semicrystalline polymers using X-ray micro-tomography. Mater Sci Eng A Struct Mater Prop Microstruct Process 2011;528(21):6535–44.
[15] Devilliers C, Fayolle B, Laiarinandrasana L, Oberti S, Gaudichet-Maurin E. Kinetics of chlorine-induced polyethylene degradation in water pipes. Polym Degrad Stab 2011;96(7):1361–8.
[16] Devilliers C. Degradation chimique du PE et influence sur le comportement, l'endommagement et la rupture en fluage: application la durabilite des canalisations sous pression (in French). Ph.D. thesis. Mines ParisTech; 2011.
[17] Maire E, Withers PJ. Quantitative X-ray tomography. Int Mater Rev 2014;59(1):1–43.
[18] Requena G, Cloetens P, Altendorfer W, Poletti C, Tolnai D, Warchomicka F, et al. Sub-micrometer synchrotron tomography of multiphase metals using Kirkpatrick-Baez optics. Scr Mater 2009;61(7):760–3.
[19] P. Bleuet, P. Cloetens, P. Gergaud, D. Mariolle, N. Chevalier, R. Tucoulou, et al, A hard X-ray nanoprobe for scanning and projection nanotomography, Rev Sci Instrum 80(5).
[20] Landron C, Maire E, Adrien J, Suhonen H, Cloetens P, Bouaziz O. Non-destructive 3-d reconstruction of the martensitic phase in a dual-phase steel using synchrotron holotomography. Scr Mater 2012;66(12):1077–80.
[21] Dzieciol K, Borbely A, Sket F, Isaac A, Di Michiel M, Cloetens P, et al. Void growth in copper during high-temperature power-law creep. Acta Mater 2011;59(2):671–7.
[22] Pawlak A, Galeski A. Cavitation during tensile drawing of annealed high density polyethylene. Polymer 2010;51(24):5771–9.
[23] Favier V, Giroud T, Strijko E, Hiver J, G'Sell C, Hellinckx S, et al. Slow crack propagation in polyethylene under fatigue at controlled stress intensity. Polymer 2002;43(4):1375–82.
[24] Landron C, Maire E, Adrien J, Bouaziz O, Michiel MD, Cloetens P, et al. Resolution effect on the study of ductile damage using synchrotron X-ray tomography. Nucl Instrum Methods Phys Res Sect B Beam Interact Mater Atoms 2012;284(0):15–8.